Journal of Magnetic Resonance 199 (2009) 173–187

Contents lists available at ScienceDirect

Journal of Magnetic Resonance

journal homepage: www.elsevier.com/locate/jmr

CHHC and ^{1}H–^{1}H magnetization exchange: Analysis by experimental solid-state NMR and 11-spin density-matrix simulations

Mihaela Aluas [a], Carmen Tripon [b], John M. Griffin [c], Xenia Filip [a], Vladimir Ladizhansky [d], Robert G. Griffin [e], Steven P. Brown [c], Claudiu Filip [b,*]

[a] Physics Department, Babes-Bolyai University, 400084 Cluj, Romania
[b] National Institute for R&D of Isotopic and Molecular Technologies, P.O. Box 700, 400293 Cluj, Romania
[c] Department of Physics, University of Warwick, Coventry CV4 7AL, UK
[d] Department of Physics, University of Guelph, 50 Stone Road East, Guelph, Ont., Canada N1G 2W1
[e] Francis Bitter Magnet Laboratory and Department of Chemistry, Massachusetts Institute of Technology, Cambridge, MA 02139, USA

ARTICLE INFO

Article history:
Received 15 April 2009
Available online 3 May 2009

Keywords:
Solid-state NMR
MAS
CHHC
^{1}H–^{1}H dipolar coupling
Distance constraints

ABSTRACT

A protocol is presented for correcting the effect of non-specific cross-polarization in CHHC solid-state MAS NMR experiments, thus allowing the recovery of the ^{1}H–^{1}H magnetization exchange functions from the mixing-time dependent buildup of experimental CHHC peak intensity. The presented protocol also incorporates a scaling procedure to take into account the effect of multiplicity of a CH_2 or CH_3 moiety. Experimental CHHC buildup curves are presented for L-tyrosine·HCl samples where either all or only one in 10 molecules are U–^{13}C labeled. Good agreement between experiment and 11-spin SPINEVOLUTION simulation (including only isotropic ^{1}H chemical shifts) is demonstrated for the initial buildup (t_{mix} < 100 μs) of CHHC peak intensity corresponding to an intramolecular close (2.5 Å) H–H proximity. Differences in the initial CHHC buildup are observed between the one in 10 dilute and 100% samples for cases where there is a close intermolecular H–H proximity in addition to a close intramolecular H–H proximity. For the dilute sample, CHHC cross-peak intensities tended to significantly lower values for long mixing times (500 μs) as compared to the 100% sample. This difference is explained as being due to the dependence of the limiting total magnetization on the ratio N_{obs}/N_{tot} between the number of protons that are directly attached to a ^{13}C nucleus and hence contribute significantly to the observed ^{13}C CHHC NMR signal, and the total number of ^{1}H spins into the system. ^{1}H–^{1}H magnetization exchange curves extracted from CHHC spectra for the 100% L-tyrosine·HCl sample exhibit a clear sensitivity to the root sum squared dipolar coupling, with fast buildup being observed for the shortest intramolecular distances (2.5 Å) and slower, yet observable buildup for the longer intermolecular distances (up to 5 Å).

1. Introduction

Solid-state nuclear magnetic resonance increasingly develops as an attractive tool for investigating complex molecular systems with practical relevance in biology, chemistry and materials science. For instance, structural investigations based on identifying protein intra-residue or neighboring residue ^{13}C–^{13}C (^{13}C–^{15}N) connectivities, distances, and angles are now almost routinely available from ^{13}C(^{15}N) solid-state NMR experiments optimized to work on multiply labeled samples [1–12], but constraints useful to elucidate the 3D structure of proteins [13], or to characterize supramolecular aggregates and crystal packing, are more difficult to obtain. A promising strategy for this purpose is to use the CHHC experiment [14–17], which makes use of the concept that such constraints are easier to extract using ^{1}H–^{1}H magnetization exchange, because protons are closer spaced in regions of interest (folding, or intermolecular contacts), and also more strongly dipolar coupled to each other than low γ nuclei.

^{1}H–^{1}H magnetization exchange can be directly probed in a NOESY-type ^{1}H–^{1}H spin-diffusion two-dimensional correlation experiment [18]. This has been shown for cases of small and moderately sized organic molecules, where sufficient ^{1}H resolution is obtained using fast MAS or homonuclear ^{1}H decoupling [19–24]. In a CHHC experiment (see pulse sequence in Fig. 1), ^{1}H–^{1}H magnetization exchange is probed indirectly, taking advantage of the better resolution for the X nucleus. NHHC [17], NHHN [25] and PHHP [26] implementations as well as extensions to 3D C(DQ)C(SQ)HHC and NHHCC experiments [10] have also been

* Corresponding author. Fax: +40 264 420042.
E-mail address: cfilip@itim-cj.ro (C. Filip).

1090-7807/$ - see front matter © 2009 Elsevier Inc. All rights reserved.
doi:10.1016/j.jmr.2009.04.013

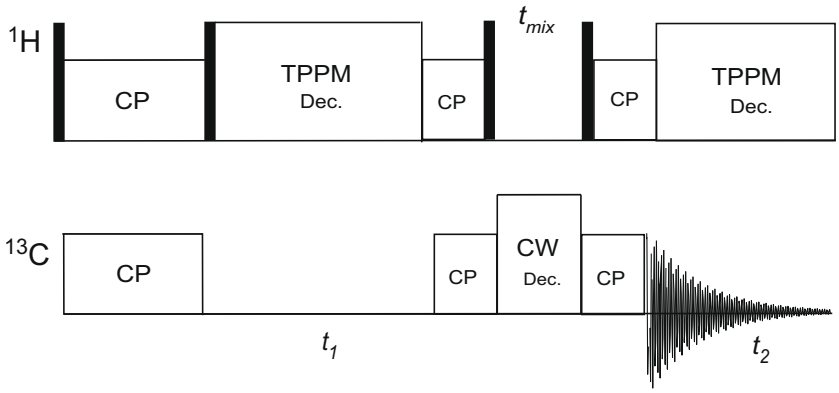

Fig. 1. The CHHC pulse sequence employed in the present work, where, in addition to previous implementations, a 60 kHz continuous-wave decoupling field is applied on the ^{13}C channel, in order to reduce the negative influence of the ^{13}C–^{1}H dipolar interaction upon the efficiency of ^{1}H–^{1}H magnetization exchange during the mixing time.

demonstrated. CHHC, NHHC and NHHN experiments are widely applied to biological systems such as microcrystalline proteins [10,17,27–32], fibrils [33–37], aggregates [38,39], chlorophylls [40–43], ion channels [44–46], RNA [47,48] and an anti-cancer agent [49], where cross peaks observed in spectra recorded with mixing times of typically at least 100 μs are used as distance constraints for structure determination protocols.

The reliability of ^{1}H–^{1}H distance constraints determined from observed cross peaks in CHHC-type experiments has been demonstrated for small model compounds, e.g., amino acids [10,15,17,25,28,50,51] as well as recently the microcrystalline CrH protein [30], where ^{1}H–^{1}H distances are known from single-crystal diffraction data. Specifically, faster experimental buildup (as a function of the mixing time, t_{mix}) of CHHC peak intensity is observed for shorter ^{1}H–^{1}H distances. Experimental CHHC buildup data has been analysed using a classical spin-diffusion model [15,16], with the extracted spin diffusion coefficients allowing order-of-magnitude estimates of ^{1}H–^{1}H distances. Reif et al. [27] and Lange et al. [50] have shown that a good fit to experimental data is obtained using analytical expressions based on $n = 0$ rotational resonance [52] and spectral spin diffusion [53,54], respectively. These expressions have a squared dependence on the dipolar coupling constant (and hence the internuclear distance) as well as a fitted phenomenological zero-quantum dephasing term, with the latter depending on the MAS frequency [50]. Elena et al. have presented a related treatment of direct ^{1}H–^{1}H magnetization exchange using a multi-spin kinetic rate matrix approach that considers a sum of all relevant magnetization processes between sites *i* and *j* in different molecules in the crystal lattice [22,23].

Advances in computing hardware and density-matrix simulation methodologies [55,56] mean that the spin dynamics due to 10+ dipolar-coupled nuclei can be simulated. For example, the dephasing in ^{13}C free-induction decays and spin-echo experiments under rotor-synchronized Hahn-echo pulse trains have recently been simulated for 10 coupled spins [57,58]. In this paper, ^{1}H–^{1}H magnetization exchange is simulated for 11-spin systems corresponding to specific proton–proton proximities in L-tyrosine·HCl, for which experimental CHHC buildup data is presented. Specifically, a protocol is introduced to correct for non-specific cross-polarization (CP) and take into account XH_n multiplicity, thus allowing a direct comparison between experimental and simulated data. The effect of inter and intramolecular ^{1}H–^{1}H proximities on ^{1}H–^{1}H magnetization exchange is investigated using two L-tyrosine·HCl samples where either all or only one in ten molecules are U–^{13}C labeled. For the all U–^{13}C sample, differences in the rate of buildup of CHHC peak intensity are explained by considering the root sum squared dipolar couplings.

2. Experimental details

2.1. Sample preparation

U (98%)–^{13}C labeled L-tyrosine was obtained from Cambridge Isotope Laboratories (Andover, MA, USA). Conversion to the L-tyrosine·HCl salt was achieved by dissolving L-tyrosine in 1 M HCl, followed by freeze-drying using a vacuum-pump. Two samples were used in this study: U–^{13}C L-tyrosine·HCl refers to the sample as prepared above. A second sample was prepared by the recrystallization of the U–^{13}C labeled L-tyrosine with natural abundant L-tyrosine in 1 M HCl, so as to yield a U–$^{13}C^{dil_10\%}$ L-tyrosine·HCl sample, i.e., one in 10 L-tyrosine·HCl molecules are fully ^{13}C labeled.

2.2. NMR experiments

Experiments were performed at room temperature on a Bruker AVANCE-400 spectrometer operating at a ^{13}C Larmor frequency of 100 MHz, at an MAS frequency of 10.5 kHz using a Bruker 4 mm double-resonance probe.

In all experiments, CP transfer was optimized for the first Hartmann–Hahn matching condition ($\nu_{1C} = \nu_{1H} - \nu_R$), using ^{1}H and ^{13}C *rf* nutation frequencies of 51 and 40 kHz, respectively. For $\pi/2$ ^{1}H *rf* pulses, a $\pi/2$ pulse length of 3.8 μs was used. During ^{13}C evolution periods, two-pulse phase-modulated (TPPM) ^{1}H decoupling [59] was applied at a nutation frequency of 70 kHz ($\Delta\varphi = 15°$ and pulse width of 7.4 μs). A recycle delay of 3 s was used.

The CHHC experiments were performed by using the pulse sequence depicted in Fig. 1, where the unwanted proton polarization left after the first CP contact pulse is removed by phase-cycling the second $\pi/2$ pulse on the ^{1}H channel, as introduced in Ref. [40]. A contact pulse of 700 μs was used for the first CP, whereas a much shorter contact pulse (65 μs) was employed for the next two CP steps in order to favorize polarization transfer between bonded ^{13}C–^{1}H in CH and CH_2 moieties. A 60 kHz continuous-wave decoupling field was also applied on the ^{13}C channel during the mixing time to reduce the negative effect of the ^{13}C–^{1}H dipolar interaction upon the efficiency of ^{1}H–^{1}H polarization transfer. 256 (U–$^{13}C^{dil\_10\%}$ sample) and 32 (U–^{13}C sample) transients were co-added for each of 256 t_1 increments of 30 μs, corresponding to a F_1 spectral width of 16.6 kHz which was chosen such as to fit only the six protonated ^{13}C resonances of interest. Sign discrimination in t_1 was achieved using the TPPI method. Total acquisition times for each 2D CHHC experiment were 54 and 7 h for the U–$^{13}C^{dil\_10\%}$ and U–^{13}C samples, respectively. The signal to noise ratio in the first row of the CHHC experiment for $t_{mix} = 0$ was better than

75:1 (U–$^{13}C^{dil\_10\%}$) and 120:1 (U–^{13}C samples) for all centre band protonated ^{13}C resonances.

2.3. Density-matrix simulations

Density-matrix simulations of ^1H–^1H magnetization exchange during the t_{mix} period of a CHHC experiment were performed using the SPINEVOLUTION program [55] for 10 kHz MAS and a ^1H Larmor frequency of 400 MHz. 11-spin systems based upon the proton coordinates as extracted from the crystal structure of L-tyrosine·HCl [60] were considered, using experimental ^1H isotropic chemical shift values (see the representative SPINEVOLUTION input files in the Appendix). It was verified that the number of crystallite orientations used was sufficient to ensure convergence. ^1H CSAs were neglected – in separate simulations, it was found that small changes to the magnetization exchange curves only started to occur for CSA anisotropies in excess of 40 ppm (for L-alanine, the largest calculated ^1H CSA has an anisotropy of 17 ppm [58]). Each simulation directly provides the magnetization exchange curves that correspond to the transfer from an initially polarized ^1H site to all the chemically distinct proton sites in the system, and took approximately 120 h on an *Opteron* Linux workstation.

3. Theory

3.1. Magnetization exchange

The transfer of z magnetization between two dipolar coupled ^1H nuclei j and k during a mixing time, t_{mix}, under the spin-diffusion operator $\hat{U}$ is described here by a polarization transfer function, $F_{jk}(t_{mix})$:

$$F_{jk}(t_{mix}) = \left\langle I_z^k \middle| \hat{U}(t_{mix}) \middle| I_z^j \right\rangle \tag{1}$$

In a CHHC experiment, a general ^{13}C–^{13}C SQ–SQ correlation is established between a $^{13}C^L H_p$ and a $^{13}C^M H_q$ resonance, via ^1H–^1H magnetization exchange between p ^1H nuclei attached to $^{13}C^L$ and q ^1H nuclei attached to $^{13}C^M$. In such a case, it is convenient to define modified polarization transfer functions for the case of unlike and like spins, i.e., corresponding to off-diagonal and diagonal peaks in a 2D CHHC spectrum:

$$F'_{LM}(t_{mix}) = \frac{1}{pq}\left\langle \sum_{k=1}^{q} I_{kz}^M \middle| \hat{U}(t_{mix}) \middle| \sum_{j=1}^{p} I_{jz}^L \right\rangle \tag{2}$$

$$F'_{LL}(t_{mix}) = \frac{1}{p}\left\langle \sum_{j=1}^{p} I_{jz}^L \middle| \hat{U}(t_{mix}) \middle| \sum_{j=1}^{p} I_{jz}^L \right\rangle \tag{3}$$

The modified polarization transfer functions correspond to ^1H–^1H magnetization exchange starting from unit polarization on a given $^{13}C^L H_p$ group. For $t_{mix} = 0$, $F'_{LL}(0) = 1$ and $F'_{LM}(0) = 0$.

In this paper, a normalized polarization transfer function is employed according to the definition:

$$F^n_{LM}(t_{mix}) = \frac{F'_{LM}(t_{mix})}{F'_{LL}(0)} \tag{4}$$

3.2. Compensating heteronuclear effects in CHHC experiments

The indirect observation of ^1H–^1H magnetization exchange in a 2D CHHC experiment benefits from the considerably better ^{13}C as opposed to ^1H resolution. However, the two CP steps flanking the ^1H–^1H magnetization exchange period in the CHHC sequence are usually not fully specific even for the very short CP durations typically used (<100 μs), i.e., magnetization is not transferred exclusively from a given ^{13}C nucleus to only its directly attached ^1H nucleus or nuclei, but rather magnetization "leaks out" onto other ^1H nuclei. As a consequence, the intensity of an experimental CHHC cross peak linking a $^{13}C^L H_p$ and a $^{13}C^M H_q$ resonance, $I^{ex}_{LM}(t_{mix})$, does not correspond precisely to the ^1H–^1H polarization transfer functions described above. This section describes a procedure for recovering the ^1H–^1H polarization transfer functions from the experimental CHHC cross-peak intensities.

The intensity of an experimental CHHC cross peak linking a $^{13}C^L H_p$ and a $^{13}C^M H_q$ resonance, $I^{ex}_{LM}(t_{mix})$, corresponds to:

$$I^{ex}_{LM}(t_{mix}) = a^L_{CP1}\left\langle S^M_{xy} \middle| \hat{U}_{IS}(\tau_{CP})\hat{U}(t_{mix})\hat{U}_{SI}(\tau_{CP}) \middle| S^L_{xy} \right\rangle \tag{5}$$

Note that S and I refer to ^{13}C and ^1H nuclei, respectively. The a^L_{CP1} coefficient takes into account the variation of initial (i.e., at the start of t_1) ^{13}C transverse magnetization for different ^{13}C resonances arising from the first CP step. The xy subscript indicates spin S transverse magnetization present at the end of t_1 or the start of t_2. The CP propagators in Eq. (5) are considered to include the contact pulse applied to both spin species and the ^1H 90° pulse that creates I_z (^1H population state) at the start of t_{mix} or converts I_z at the end of t_{mix} into ^1H transverse magnetization before the final CP step, i.e., $\hat{U}_{SI}(\tau_{CP})$ converts S_{xy} into I_z, while $\hat{U}_{IS}(\tau_{CP})$ converts I_z into S_{xy}. The CP dynamics can be described in terms of the transferred polarization:

$$\hat{U}_{SI}(\tau_{CP})\left| S^L_{xy} \right\rangle \;\rightarrow\; \frac{\eta_L}{p}\left| \sum_{j=1}^{p} I^L_{jz} \right\rangle + \frac{\varepsilon_{LM}}{q}\left| \sum_{k=1}^{q} I^M_{kz} \right\rangle \tag{6}$$

where the coefficient η corresponds to the amount of magnetization transferred to proton(s) directly attached to the initial ^{13}C resonance, while the coefficient ε corresponds to the amount of magnetization transferred to proton(s) attached to a different ^{13}C resonance. Similarly,

$$\left\langle S^M_{xy} \middle| \hat{U}_{IS}(\tau_{CP}) \;\rightarrow\; \left\langle \sum_{k=1}^{q} I^M_{kz} \right| \frac{\eta_M}{q} + \left\langle \sum_{j=1}^{p} I^L_{jz} \right| \frac{\varepsilon_{ML}}{p} \tag{7}$$

It thus follows that

$$\begin{aligned} I^{ex}_{LM}(t_{mix}) = {} & a^L_{CP1}\eta_L\eta_M \frac{\left\langle \sum_{k=1}^{q} I^M_{kz} \middle| \hat{U}(t_{mix}) \middle| \sum_{j=1}^{p} I^L_{jz} \right\rangle}{pq} \\ & + \frac{a^L_{CP1}\eta_M\varepsilon_{LM}}{q} \frac{\left\langle \sum_{k=1}^{q} I^M_{kz} \middle| \hat{U}(t_{mix}) \middle| \sum_{k=1}^{q} I^M_{kz} \right\rangle}{q} \\ & + \frac{a^L_{CP1}\eta_L\varepsilon_{ML}}{p} \frac{\left\langle \sum_{j=1}^{p} I^L_{jz} \middle| \hat{U}(t_{mix}) \middle| \sum_{j=1}^{p} I^L_{jz} \right\rangle}{p} \end{aligned} \tag{8}$$

where the term in $\varepsilon_{LM}\,\varepsilon_{ML}$ has been neglected.

The intensity of an experimental CHHC diagonal peak for a $^{13}C^L H_p$ resonance, $I^{ex}_{LL}(t_{mix})$, corresponds to:

$$I^{ex}_{LL}(t_{mix}) = a^L_{CP1}\left\langle S^L_{xy} \middle| \hat{U}_{IS}(\tau_{CP})\hat{U}(t_{mix})\hat{U}_{SI}(\tau_{CP}) \middle| S^L_{xy} \right\rangle \tag{9}$$

where

$$\left\langle S^L_{xy} \middle| \hat{U}_{IS}(\tau_{CP}) \;\rightarrow\; \left\langle \sum_{j=1}^{p} I^L_{jz} \right| \frac{\eta_L}{p} + \left\langle \sum_{k=1}^{q} I^M_{kz} \right| \frac{\varepsilon_{LM}}{q} \tag{10}$$

i.e.,

$$\begin{aligned} I^{ex}_{LL}(t_{mix}) = {} & \frac{a^L_{CP1}\eta_L^2}{p} \frac{\left\langle \sum_{j=1}^{p} I^L_{jz} \middle| \hat{U}(t_{mix}) \middle| \sum_{j=1}^{p} I^L_{jz} \right\rangle}{p} \\ & + a^L_{CP1}\eta_L\varepsilon_{LM} \frac{\left\langle \sum_{j=1}^{p} I^L_{jz} \middle| \hat{U}(t_{mix}) \middle| \sum_{k=1}^{q} I^M_{kz} \right\rangle}{pq} \\ & + a^L_{CP1}\eta_L\varepsilon_{LM} \frac{\left\langle \sum_{k=1}^{q} I^M_{kz} \middle| \hat{U}(t_{mix}) \middle| \sum_{j=1}^{p} I^L_{jz} \right\rangle}{pq} \end{aligned} \tag{11}$$

where the term in $\varepsilon_{LM}{}^2$ has been neglected.

Using Eqs. (2) and (3), Eqs. (8) and (11) become:

$$I^{ex}_{LM}(t_{\rm mix}) = a^L_{CP1}\left[\eta_L\eta_M F'_{LM}(t_{\rm mix}) + \frac{\eta_M\varepsilon_{LM}}{q}F'_{MM}(t_{\rm mix}) + \frac{\eta_L\varepsilon_{ML}}{p}F'_{LL}(t_{\rm mix})\right] \quad (12)$$

$$I^{ex}_{LL}(t_{\rm mix}) = a^L_{CP1}\left[\frac{\eta^2_L}{p}F'_{LL}(t_{\rm mix}) + \eta_L\varepsilon_{LM}F'_{ML}(t_{\rm mix}) + \eta_L\varepsilon_{LM}F'_{LM}(t_{\rm mix})\right] \quad (13)$$

For a short $t_{\rm mix}$, $F'_{ML}(t_{\rm mix})$ and $F'_{LM}(t_{\rm mix})$ are both small, while for a short τ_{CP}, ε_{LM} and ε_{ML} are also small. For such conditions, Eq. (13) simplifies to

$$I^{ex}_{LL}(t_{\rm mix}) = \frac{a^L_{CP1}\eta^2_L}{p}F'_{LL}(t_m) \quad (14)$$

i.e.,

$$F'_{LL}(t_{\rm mix}) = \frac{p}{a^L_{CP1}\eta^2_L}I^{ex}_{LL}(t_{\rm mix}) \quad (15)$$

Eq. (12) can, then, be reexpressed as

$$\begin{aligned} I^{ex}_{LM}(t_{\rm mix}) &= a^L_{CP1}\eta_L\eta_M F'_{LM}(t_{\rm mix}) + \frac{\eta_M\varepsilon_{LM}}{q}\frac{q}{\eta^2_M}I^{ex}_{MM}(t_{\rm mix}) + \frac{\eta_L\varepsilon_{ML}}{p}\frac{p}{\eta^2_L}I^{ex}_{LL}(t_{\rm mix}) \\ &= a^L_{CP1}\eta_L\eta_M F'_{LM}(t_{\rm mix}) + \frac{\varepsilon_{LM}}{\eta_M}I^{ex}_{MM}(t_{\rm mix}) + \frac{\varepsilon_{ML}}{\eta_L}I^{ex}_{LL}(t_{\rm mix}) \end{aligned} \quad (16)$$

By analogy

$$I^{ex}_{ML}(t_{\rm mix}) = a^M_{CP1}\eta_L\eta_M F'_{ML}(t_{\rm mix}) + \frac{\varepsilon_{ML}}{\eta_L}I^{ex}_{LL}(t_{\rm mix}) + \frac{\varepsilon_{LM}}{\eta_M}I^{ex}_{MM}(t_{\rm mix}) \quad (17)$$

The differences between Eqs. (16) and (17) explain why L to M and M to L cross peaks in CHHC experiments can exhibit different intensities for non-zero $t_{\rm mix}$.

Rearranging Eq. (16),

$$F'_{LM}(t_{\rm mix}) = \frac{1}{a^L_{CP1}\eta_L\eta_M}\left[I^{ex}_{LM}(t_{\rm mix}) - \frac{\varepsilon_{LM}}{\eta_M}I^{ex}_{MM}(t_{\rm mix}) - \frac{\varepsilon_{ML}}{\eta_L}I^{ex}_{LL}(t_{\rm mix})\right] \quad (18)$$

Using Eqs. (15) and (18), the normalized polarization transfer function defined in Eq. (4) is given as:

$$F^n_{LM}(t_{\rm mix}) = \frac{F'_{LM}(t_{\rm mix})}{F'_{LL}(0)} = f_{LM}\left(\frac{I^{ex}_{LM}(t_{\rm mix}) - \frac{\varepsilon_{LM}}{\eta_M}I^{ex}_{MM}(t_{\rm mix}) - \frac{\varepsilon_{ML}}{\eta_L}I^{ex}_{LL}(t_{\rm mix})}{I^{ex}_{LL}(0)}\right) \quad (19)$$

where

$$f_{LM} = \frac{\eta_L}{p\eta_M} \quad (20)$$

Eq. (19) defines how the normalized polarization transfer functions – corresponding to only ^{1}H–^{1}H magnetization exchange, i.e., with no distorting effect from non-specific CP – can be extracted from the experimental CHHC cross-peak intensities.

The following describes how the coefficients in Eq. (19) can be experimentally determined. Using the above theoretical model (see Eq. (14)), the ratio β_L of the intensity of a specific ^{13}C resonance recorded in a CHHC filtered spectrum (obtained by using the CHHC pulse sequence with t_1 and $t_{\rm mix}$ set to zero), a^L_{CHHC}, and that acquired after the first CP step, a^L_{CPI} can be related to the corresponding CP transfer parameter, η_L, and proton multiplicity, through:

$$\beta_L = \frac{a^L_{CHHC}}{a^L_{CP1}} = \frac{\eta^2_L}{p} \quad (21)$$

It then follows that

$$\eta_L = \sqrt{p\beta_L} \quad (22)$$

By inserting this in Eq. (20) the following expression is obtained for the f_{LM} coefficient

$$f_{LM} = \frac{1}{\sqrt{pq}}\sqrt{\frac{\beta_L}{\beta_M}} \quad (23)$$

which provides the desired dependence only on the experimentally determined parameters β_L and β_M.

For $t_{\rm mix} = 0$, $F'_{LM}(t_{\rm mix}) = F'_{ML}(t_{\rm mix}) = 0$, and hence Eq. (16) becomes

$$I^{ex}_{LM}(0) = I^{ex}_{ML}(0) = \frac{\varepsilon_{ML}}{\eta_L}I^{ex}_{LL}(0) + \frac{\varepsilon_{LM}}{\eta_M}I^{ex}_{MM}(0) \quad (24)$$

Within the approximation that $\varepsilon = \varepsilon_{LM} = \varepsilon_{ML}$, ε can be determined:

$$\varepsilon_{LM} = \frac{I^{ex}_{LM}(0)}{\left[\frac{I^{ex}_{LL}(0)}{\eta_L} + \frac{I^{ex}_{MM}(0)}{\eta_M}\right]} \quad (25)$$

where η_L and η_M are determined using Eq. (22).

The above calculation is for the case where all carbon nuclei are ^{13}C, i.e., where all molecules are U–^{13}C labeled. For a dilute sample, which corresponds to the case where only a proportion ρ of the molecules are U–^{13}C labeled, it is necessary to correct for the contribution to the diagonal peak intensity of the natural abundance ^{13}C nuclei (denoted here as ξ, with $\xi = 0.011$ for ^{13}C) in the proportion $(1-\rho)$ of the molecules at natural abundance. This correction is required since only ξ^2 molecules will have two neighboring ^{13}C-labeled atoms, so as to give rise to cross-peak intensity $I^{ex}_{LM}(0)$, as compared to the ξ molecules that have a single ^{13}C-labeled atom that contributes to the diagonal peak intensity. Considering the diagonal peak intensity, $I^{ex}_{LL}(0)$, there is a contribution $\xi\ (1-\rho)$ from molecules at natural abundance in addition to the ρ from the U–^{13}C labeled molecules. It is hence necessary to modify Eq. (25)

$$\varepsilon_{LM} = \frac{I^{ex}_{LM}(0)}{\left[\frac{\lambda I^{ex}_{LL}(0)}{\eta_L} + \frac{\lambda I^{ex}_{MM}(0)}{\eta_M}\right]} \quad (26)$$

where

$$\lambda = \frac{\rho}{\rho + \xi(1-\rho)} \quad (27)$$

i.e., for ^{13}C, $\lambda = 0.91$ when $\rho = 0.1$. Eq. (26) does not include a correction to the cross-peak intensity $I^{ex}_{LM}(0)$ which is given by $\rho/[\rho + \xi^2(1-\rho)]$, since this equals 1.00 to two decimal places for ^{13}C when $\rho = 0.1$.

For a dilute sample, it is also necessary to modify Eq. (19):

$$F^n_{LM}(t_{\rm mix}) = \frac{F'_{LM}(t_{\rm mix})}{F'_{LL}(0)} = f_{LM}\left(\frac{I^{ex}_{LM}(t_{\rm mix}) - \frac{\varepsilon_{LM}}{\eta_M}\lambda I^{ex}_{MM}(t_{\rm mix}) - \frac{\varepsilon_{ML}}{\eta_L}\lambda I^{ex}_{LL}(t_{\rm mix})}{\lambda I^{ex}_{LL}(0)}\right) \quad (28)$$

4. Results and discussion

4.1. One-dimensional ^{13}C CP MAS and CHHC-filtered spectra

Fig. 2 compares ^{13}C CP MAS (thin line) and ^{13}C CHHC-filtered ($t_1 = t_{\rm mix} = 0$, $\tau_{CP} = 65$ μs for the last two CP steps) spectra (thick line) for (a) U–^{13}C and (b) U–^{13}C$^{\rm dil_10\%}$ L-tyrosine·HCl. The η_L CP transfer coefficients as determined from a comparison of the signal intensity in the CP MAS and CHHC-filtered experiments (see Eqs. (21) and (22)) are listed in Table 1.

4.2. Two-dimensional CHHC spectra

Fig. 3 presents 2D CHHC ($\tau_{CP} = 65$ μs for the last two CP steps) spectra of (a and b) U–^{13}C and (c and d) U–^{13}C$^{\rm dil_10\%}$ L-tyrosine·HCl recorded with $t_{\rm mix}$ equal to (a and c) 0 and (b and d) 100 μs. Fig. 4 presents rows through the F_1 resonances corresponding to the six

protonated ^{13}C nuclei, as extracted from the CHHC spectra at zero mixing time. It is evident that non-specific CP during the last two CP steps of the CHHC experiment gives rise to noticeable CHHC cross peaks between directly bonded ^{13}C nuclei (i.e., 2 and 4, 3 and 5, and 7 and 8), even for the case of zero mixing time. This is also evident in Fig. 5(a) and (b) which presents the buildup of C7 (βCH_2) to C8 (αCH) (open symbols) and C8 to C7 (filled symbols) cross-peak intensity as a function of t_{mix} for (a) U–^{13}C and (b) U–$^{13}C^{dil\_10\%}$ L-tyrosine·HCl. Specifically, the cross-peak intensities are normalized with respect to the intensity of the corresponding diagonal peak for zero mixing time, i.e., $I^{ex}_{LM}(t_{mix})/I^{ex}_{LL}(0)$ such that the C7–C8 and C8–C7 cross-peak intensities are divided by the intensity of the C7 and C8 diagonal peak intensity for zero mixing time, respectively. In the case of the U–$^{13}C^{dil\_10\%}$ sample, a scaling by the factor λ as defined in Eq. (27) of 0.91 was applied to $I^{ex}_{LL}(0)$.

Table 1
The experimental η_L parameters evaluated using Eqs. (21) and (22) for the specified $^{13}C^L$ sites in L-tyrosine·HCl.

	η_L (U–^{13}C)	η_L (U–$^{13}C^{10\%\_dil}$)
C7	0.66 ± 0.01	0.63 ± 0.03
C8	0.52 ± 0.01	0.50 ± 0.02
C2	0.51 ± 0.01	0.51 ± 0.03
C3	0.52 ± 0.01	0.51 ± 0.02
C5	0.55 ± 0.02	0.54 ± 0.03
C4	0.53 ± 0.01	0.52 ± 0.04

Section 3.2 (see Eqs. (19) and (28)) describes a procedure for recovering the ^1H–^1H magnetization exchange behavior given by $F^n_{LM}(t_{mix})$ from the experimental CHHC buildup curves. Fig. 5(c) and (d) presents such corrected normalized buildup plots for the C7–C8 and C8–C7 cross peaks for (c) U–^{13}C and (d) U–$^{13}C^{dil\_10\%}$

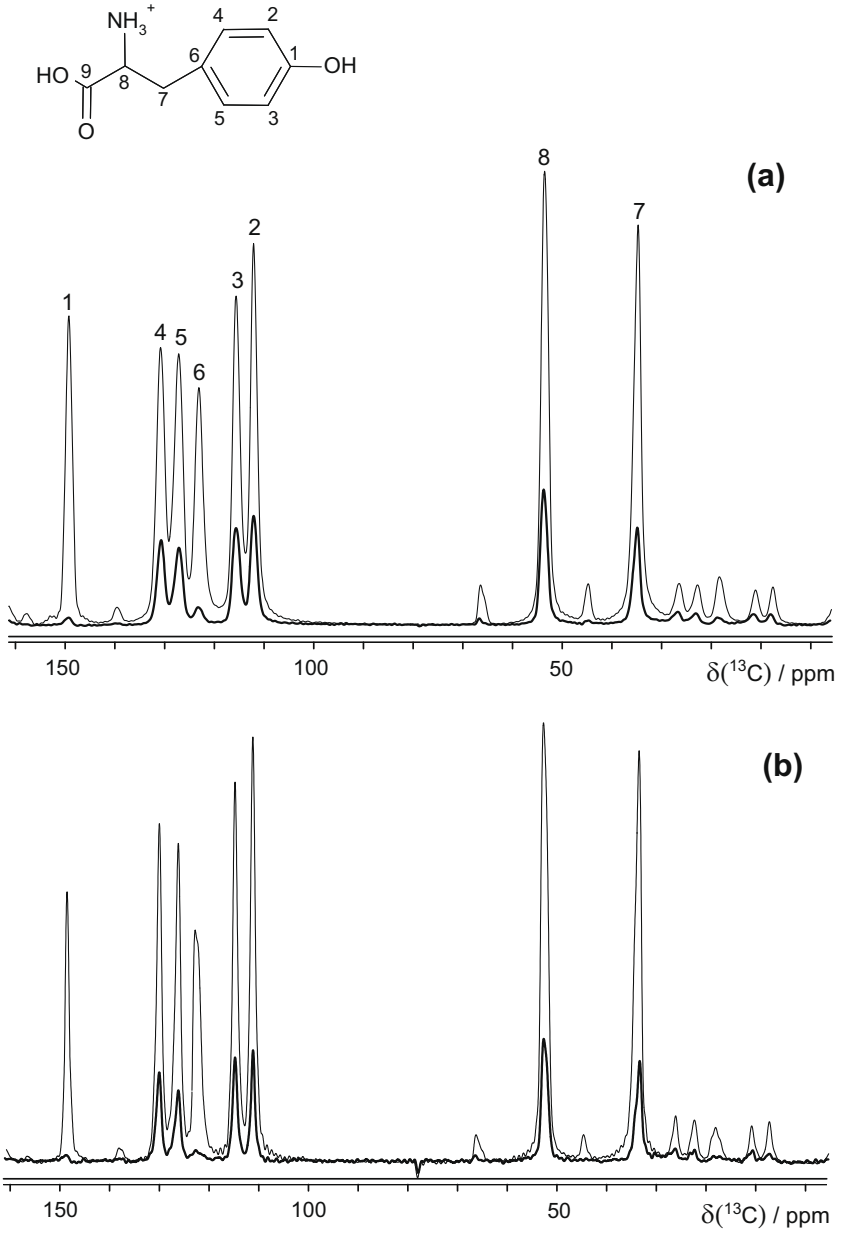

Fig. 2. A comparison of ^{13}C CP MAS (thin line) and ^{13}C CHHC-filtered ($t_1 = t_{mix} = 0$, $\tau_{CP} = 65$ μs for the last two CP steps) spectra (thick line) for (a) U–^{13}C and (b) U–$^{13}C^{dil\_10\%}$ L-tyrosine·HCl. The contact pulse for the first CP step in the CHHC experiment (and the only CP step in the CP MAS experiment) was of duration 700 μs. For both experiments, 32 (U–^{13}C) and 256 (U–$^{13}C^{dil\_10\%}$) transients were co-added for a recycle delay of 3 s.

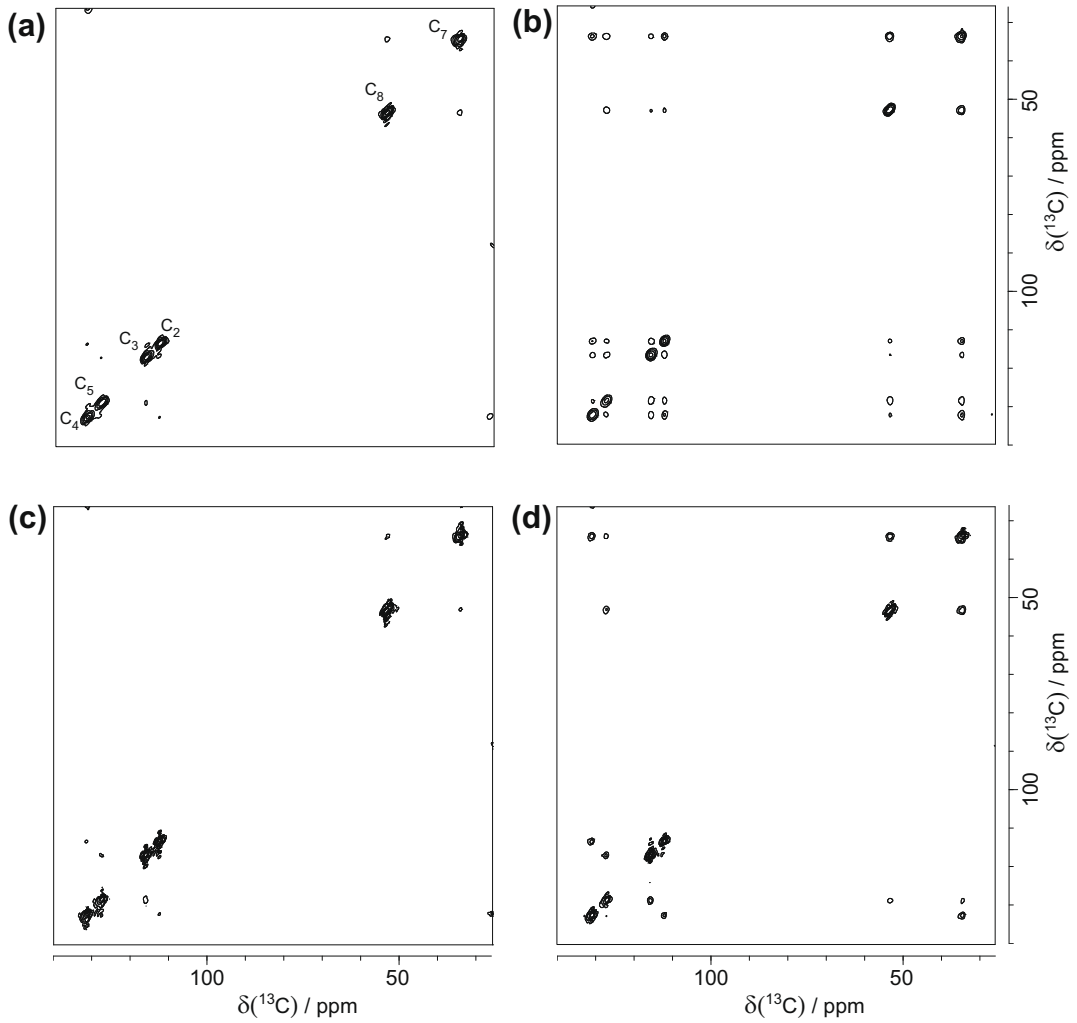

Fig. 3. 2D CHHC spectra of (a and b) U–^{13}C and (c and d) U–$^{13}C^{dil_10\%}$ L-tyrosine·HCl recorded with t_{mix} equal to (a and c) 0 and (b and d) 100 μs. The base contour level is at 3% and 5% for the two different mixing times.

L-tyrosine·HCl. In the evaluation of the ε_{LM} coefficients (see Eqs. (25) and (26)), the coefficient was set to zero when $I^{ex}_{LM}(t_{mix})/I^{ex}_{LL}(0) < 0.01$, i.e., when a particular cross-peak was less than 1% of the intensity of the corresponding diagonal peak. The evaluated non-zero ε_{LM} coefficients for the different CHHC cross peaks are listed in Table 2. Considering Fig. 5(c) and (d), it is evident that all corrected curves now start at zero. As shown below, this allows for a clear comparison with the ^{1}H–^{1}H magnetization exchange buildup behavior obtained from numerical density-matrix simulations. The corrected experimental C7 to C8 and C8–C7 transfer functions are observed to be the same within (or close to within) the experimental error bars. In the following, experimental $F^n_{LM}(t_{mix})$ values for a C^L, C^M pair are shown as an average of $F^n_{LM}(t_{mix})$ and $F^n_{ML}(t_{mix})$.

4.3. Comparison of experimental and simulated CHHC buildup curves

Corrected normalized buildup plots, i.e., $F^n_{LM}(t_{mix})$, for U–^{13}C (circles) and U–$^{13}C^{dil_10\%}$ (triangles) L-tyrosine·HCl are shown in Fig. 6 for the (a) C7–C8 and (b) C2–C4 CHHC cross peaks. The experimental data is compared to a SPINEVOLUTION simulation (solid line) of the $F^n_{LM}(t_{mix})$ ^{1}H–^{1}H magnetization function defined in Eq. (4) for 11-spin systems centered around the H7 (two protons) and H8 and H2 and H4 ^{1}H nuclei, as shown in Fig. 6(c) and (d). Inter-proton distances for the 11-spin systems are given in Tables 3 and 4.

Comparing the experimental data in Fig. 6(a) and (b) with the simulated 11-spin ^{1}H–^{1}H magnetization exchange curves, while there is good agreement for short t_{mix} (<100 μs), it is noticeable that the experimental data for the U–$^{13}C^{dil\_10\%}$ sample, in particular, trends to a markedly lower value than that for the simulation at long mixing times. For the diluted sample, the unlabeled molecules located around a fully ^{13}C-labeled molecule can be viewed as a proton bath where a significant amount of the initial polarization is lost, because it cannot be back-transferred to observable ^{13}C NMR signal during the last CP block. This is responsible for the much stronger attenuation of the CHHC cross-peak intensities at large mixing times in the 10%-diluted sample compared to the 100% sample. Quantitatively, the efficiency loss by this mechanism is illustrated in Fig. 7. Specifically, Fig. 7 compares for the U–^{13}C (circles) and U–$^{13}C^{dil_10\%}$ (triangles) L-tyrosine·HCl samples the evolution with the mixing time of the total observable experimental polarization that originates from an initial unit C7 polarization. This is defined as the sum of the normalized I_{C7} diagonal peak intensity and the intensities $I_{C7,Cj}$ within its associated cross-peak patterns (corrected by the procedure described above, i.e., $F^n_{LM}(t_{mix})$), with j = 2, 3, 4, 5 and 8. Considering that an equal distribution of ^{1}H polarization is obtained at large mixing times, and neglecting spin-lattice relaxation, an asymptotic evolution would be expected towards a saturation level given by the ratio N_{obs}/N_{tot} between the number of protons that are directly attached to a ^{13}C

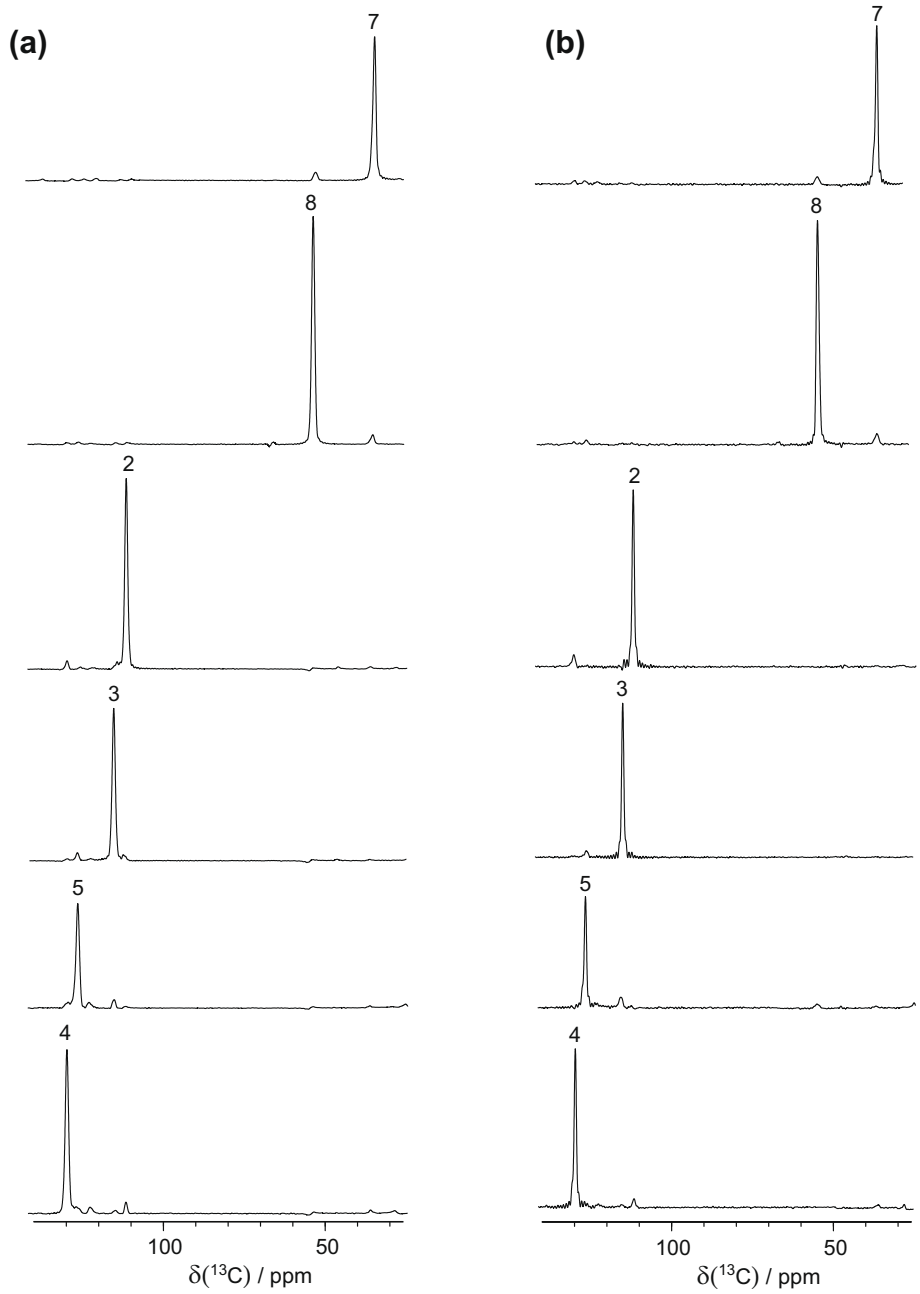

Fig. 4. Rows extracted from the 2D CHHC spectra (see Fig. 3(a) and (c)) of (a) U–^{13}C and (b) U–$^{13}C^{dil_10\%}$ L-tyrosine·HCl recorded with t_{mix} equal to 0 μs.

nucleus and hence contribute significantly to the observed ^{13}C NMR signal, and the total number of ^{1}H spins into the system. Its value is N_{obs}/N_{tot} = 7/12 = 0.58 (NB: there are 7 CH and CH_2 protons and 5 NH_3 and OH protons in the L-tyrosine·HCl molecule) and 7/120 = 0.06 in the case of the U–^{13}C and U–$^{13}C^{dil_10\%}$ samples, respectively. As can be seen in Fig. 7, the experimental total polarization trends towards these N_{obs}/N_{tot} values.

Considering the experimental data in Fig. 6(a) and (b), differences are apparent for short mixing times (t_{mix} < 100 μs) when comparing the buildup for the U–^{13}C (circles) and U–$^{13}C^{dil_10\%}$ (triangles) samples for (a) the C7 (CH_2) and C8 (αCH) and (b) the C2 and C4 (directly bonded aromatic carbons) CHHC cross peaks. Specifically, in Fig. 6(a), the observed buildup rate is faster for the U–^{13}C sample, while in Fig. 6(b), the buildup is the same within the experimental noise for the U–^{13}C and U–$^{13}C^{dil_10\%}$ samples. This is a consequence of additional close intermolecular proximities for the H7, H8 case: the intra and intermolecular contributions to the total C7, C8 cross-peak buildup curve are of comparable magnitudes, as they correspond to H7–H8 inter-proton average distances of 2.8 and 3.2 Å, respectively (see Table 3). By comparison, for the H2, H4 case, the nearest intermolecular proximity is 4.5 Å as compared to the intramolecular proximity of 2.5 Å (see Table 4). The 11-spin SPINEVOLUTION simulations (solid line in Fig. 6(a) and (b)) only consider intramolecular ^{1}H–^{1}H magnetization transfer – for H7, H8, see footnote d of Table 3 and the representative SPINEVOLUTION input files in the Appendix. Good agreement between experiment and simulation for short mixing times (<80 μs) is obtained for the C7, C8 buildup curve for the U–$^{13}C^{dil_10\%}$ sample (triangles in Fig. 6(a)) and for the C2, C4 buildup curves in Fig. 6(b) for both samples, i.e., for those cases where intermolecular proximities do not contribute to the experimentally detected ^{1}H–^{1}H magnetization exchange. The deviations between experiment and

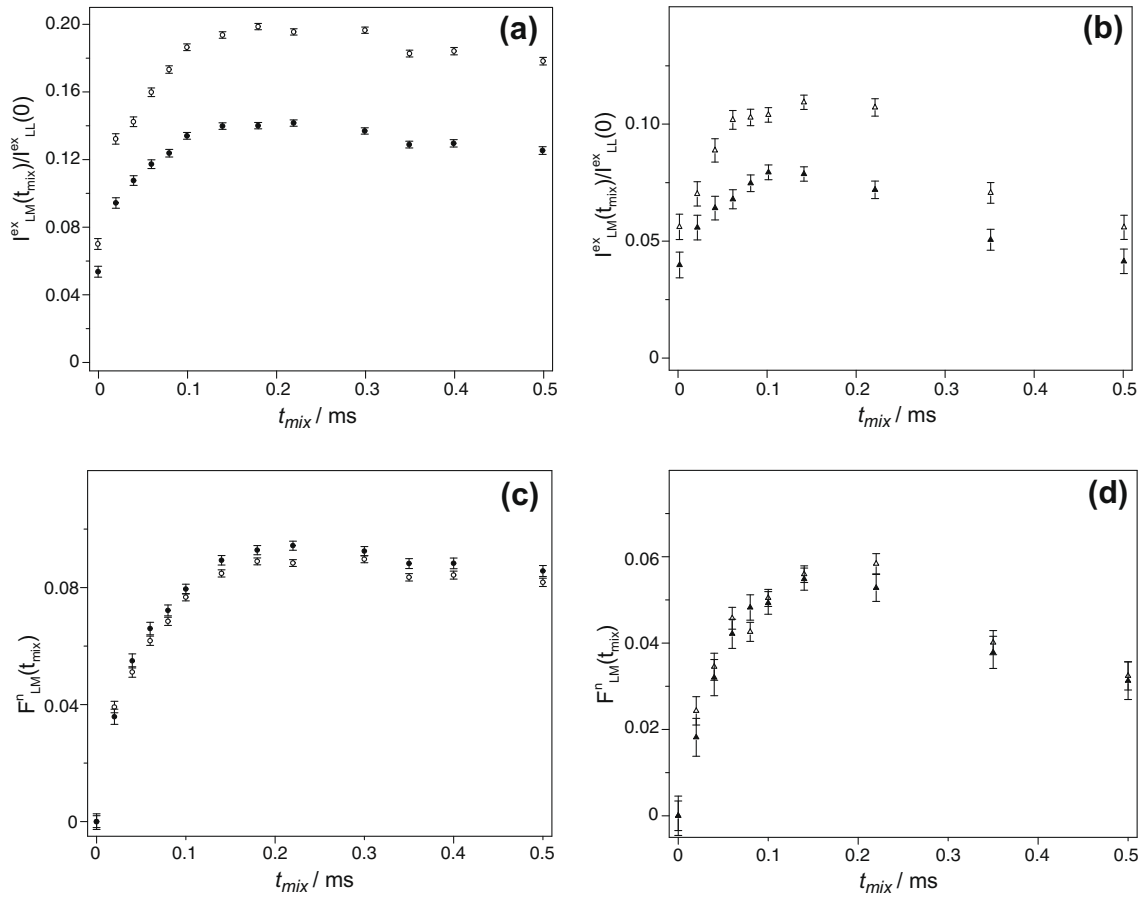

Fig. 5. The buildup of C7 (βCH_2) to C8 (αCH) (open symbols) and C8–C7 (filled symbols) cross-peak intensity as a function of t_{mix} for (a and c) U–^{13}C and (b and d) U–$^{13}C^{dil_10\%}$ L-tyrosine·HCl. In (a) and (b), the cross-peak intensities are normalized with respect to the intensity of the corresponding diagonal peak for zero mixing time, i.e., $I^{ex}_{LM}(t_{mix})/I^{ex}_{LL}(0)$. In the case of the U–$^{13}C^{dil\_10\%}$ sample, a scaling by the factor λ as defined in Eq. (27) of 0.91 was applied to $I^{ex}_{LL}(0)$. (c) and (d): corrected normalized buildup plots given by $F^{n}_{LM}(t_{mix})$ as defined in Eqs. (19) and (28) of Section 3.2. Tables 1 and 2 list the η_L and ε_{LM} coefficients.

Table 2
The ε_{LM} coefficients as evaluated using Eqs. (25) and (26) for the U–^{13}C labeled (top entry), and U–$^{13}C^{10\%_dil}$ (bottom entry) L-tyrosine·HCl samples, respectively.

	C7	C8	C2	C3	C5	C4
C7	—	0.016 ± 0.002 0.014 ±0.005	0	0	0	0
C8	0.018 ± 0.003 0.015 ± 0.005	—	0	0	0	0
C2	0	0	—	0	0	0.012 ± 0.002 0.011 ± 0.003
C3	0	0	0	—	0.014 ± 0.003 0.014 ± 0.005	0
C5	0	0	0	0.017 ± 0.003 0.013 ± 0.004	—	0
C4	0	0	0.016 ± 0.002 0.014 ± 0.004	0	0	—

simulation at longer mixing times is a consequence of "loss" of magnetization experimentally to ^{1}H nuclei that are not bonded to a visible ^{13}C nucleus as discussed above (see Fig. 7).

4.4. Analysis of the effect of multiple ^{1}H–^{1}H contacts in CHHC experiments

Fig. 6 shows examples of ^{1}H magnetization exchange observed for two specific cases, namely an isolated single ^{1}H–^{1}H contact (H2, H4, Fig. 6(b)) and a relatively tight H7–H8 intermolecular pair in the close neighborhood of a short intramolecular H7–H8 pair (see Fig. 6(a) for the U–^{13}C sample). This section considers the ^{1}H magnetization exchange behavior for the different cases of ^{1}H–^{1}H contacts found in L-tyrosine·HCl. Table 5 lists all ^{1}H–^{1}H distances under 5 Å. If we define a "close" ^{1}H–^{1}H contact as a distance under 3.5 Å, the ^{1}H–^{1}H contacts corresponding to the distinct CHHC cross-peaks can be classified either with respect to the number of involved contacts, i.e., *single*- (H2–H3, H2–H4, H2–H7, H3–H5, H3–H7, H4–H5, H4–H7, H5–H8), *double*- (H2–H5, H5–H7, H7–H8), and *triple* contacts (H3–H4), or according to their type, i.e., *only intra*- (H2–H4, H3–H5, H4–H7, H5–H8), *only inter*- (H2–H3, H2–H5, H2–H7, H3–H4, H3–H7, H4–H5), and *mixed* intra and intermolecular ^{1}H–^{1}H contacts (H5–H7, H7–H8). Note that for the case of H7 that corresponds to the two CH_2 protons, proximities of the

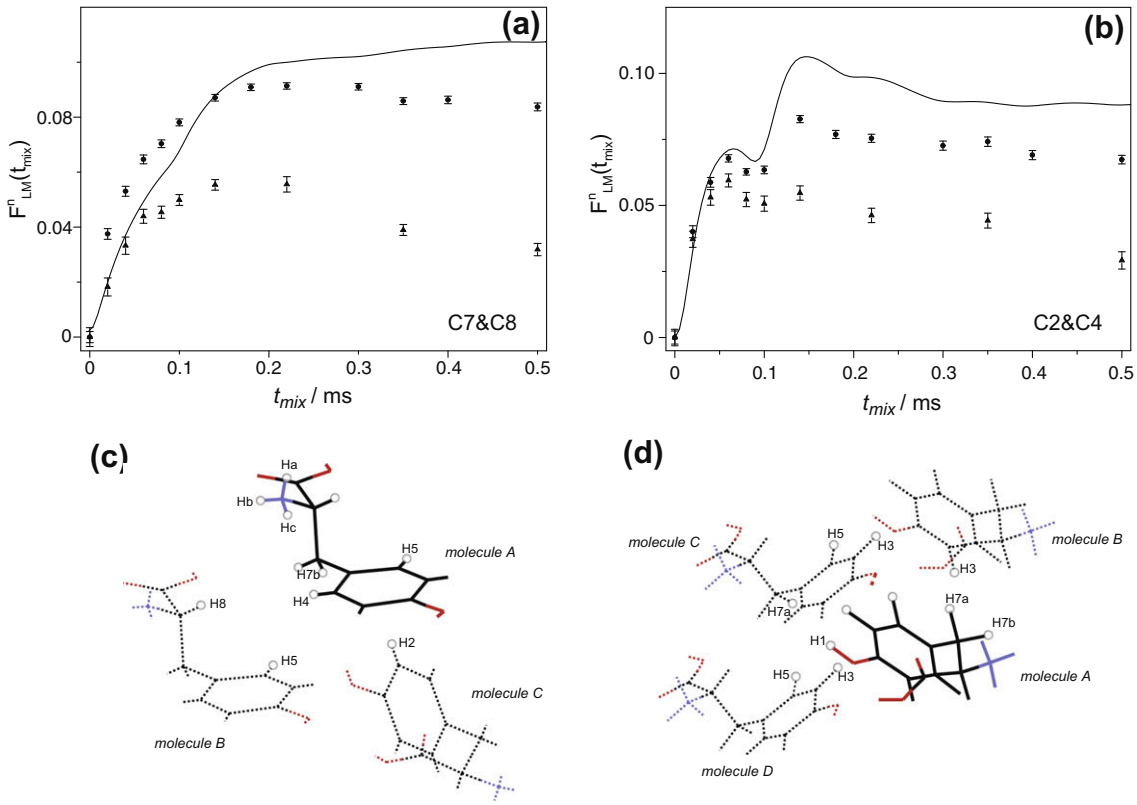

Fig. 6. Comparison between the corrected normalized experimental CHHC buildup curves, i.e., $F^n_{LM}(t_{\mathrm{mix}})$ as defined in Eqs. (19) and (28), for U–^{13}C (circles) and U–^{13}C$^{\mathrm{dil_10\%}}$ (triangles) L-tyrosine·HCl for (a) C7–C8 and (b) C2–C4. The solid lines in (a) and (b) correspond to SPINEVOLUTION density-matrix simulations of $F^n_{LM}(t_{\mathrm{mix}})$ (see Eq. (4)) for 11-spin systems centered around H7, H8 and H2, H4 ^{1}H nuclei as illustrated in (c) and (d), respectively.

Table 3
Inter-proton distances (in Angstroms) for the 11-spin system used in the SPINEVOLUTION simulations of the H7, H8 magnetization exchange[a–d].

	H2	H4	H5	NHa	NHb	NHc	H7a	H7b	H8
H7a	3.75(C)	**2.32(A)**	**3.78(A)** 2.93(B)	**3.65(A)**	2.63(A)	**2.85(A)**		**1.74(A)**	**3.06(A)** **2.93(B)**
H7b	2.31(C)	**3.5(A)**	**2.73(A)** 2.8(B)	**3.51(A)**	**3.11(A)**	2.32(A)	**1.74(A)**		**2.5(A)** 3.4(B)
H8	4.14(C)	**4.45(A)**	**2.55(A)** 5.25(B)	3.31(A)	**2.96(A)**	**2.49(A)**	**3.06(A)** 2.93(B)	**2.5(A)** 3.4(B)	5.1(B)

[a](A), (B) and (C) refer to the labeling of the molecules in Fig. 6(c).
[b]Intramolecular distances (within molecule A) are shown in bold.
[c]The closest distances to the next nearest eight ^{1}H nuclei external to the central H7 and H8 nuclei are underlined.
[d]Only intramolecular H7–H8 polarization transfer was considered in the simulations, i.e., initial density-matrix corresponds to I_z for H7a and H7b, with the read out only on H8 of molecule A. See the representative SPINEVOLUTION input files in the Appendix.

Table 4
Inter-proton distances (in Angstroms) for the 11-spin system used in the SPINEVOLUTION simulations of the H2, H4 magnetization exchange[a–c].

	H1	H2	H3	H4	H5	H7a	H7b
H2	**2.35(A)**		4.06(B) 4.30(C) 2.95(D)	**2.48(A)**	2.76(C) 3.18(D)	**4.65(A)** 2.31(C)	**5.35(A)**
H4	**4.61(A)**	**2.48(A)**	3.24(B) 2.84(C) 3.19(D)		3.07(C) 4.89(D)	**2.32(A)** 4.15(C)	**3.50(A)**

[a](A), (B), (C) and (D) refer to the labeling of the molecules in Fig. 6(d).
[b]Intramolecular distances (within molecule A) are shown in bold.
[c]The closest distances to the next nearest nine ^{1}H nuclei external to the central H2 and H4 nuclei are underlined.

same type and from the same other proton to both CH_2^a and CH_2^b are only counted once in the above classification – this is consistent with proton multiplicity being explicitly taken into account in the above analysis (see Section 3.1).

The simplest case corresponds to single ^{1}H–^{1}H intramolecular contacts, i.e., C2–C4, C3–C5, C4–C7 and C5–C8. The example of the C2–C4 CHHC buildup curves (Fig. 6(b)) has been discussed above: the observed good correspondence between the two experimental curves for the U–^{13}C and U–^{13}C$^{\mathrm{dil_10\%}}$ samples on the one hand, and between the experiment and simulation, on the other hand, are illustrative for the conditions that must be satisfied by a short 2.5 Å contact (i.e., corresponding to directly bonded CH_n moieties) that can be considered as a single contact. It is evident that the added contribution to magnetization exchange dynamics of the closest ^{1}H–^{1}H contacts can be safely neglected if they correspond to inter-proton distances larger than about ~4 Å. The identification of such intramolecular single contacts is useful in that they provide (as discussed below) reference curves for the analysis

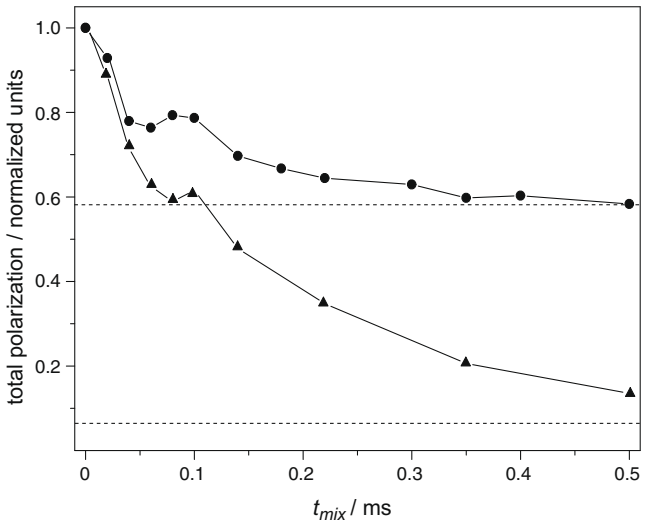

Fig. 7. The evolution with the CHHC mixing time of the total C7 polarization in the U–^{13}C (circles) and U–$^{13}C^{dil_10\%}$ (triangles) L-tyrosine·HCl samples, considering an initial state of unit polarization. The total polarization is expected to trend towards N_{obs}/N_{tot} = 7/12 = 0.58, and 7/120 = 0.06 for the U–^{13}C (circles) and U–$^{13}C^{dil_10\%}$ samples, respectively (see horizontal dashed lines).

of other buildup curves that depend on contributions from multiple contacts.

In the following, we consider experimental CHHC data for U–^{13}C L-tyrosine·HCl, where close *intermolecular* ^{1}H–^{1}H proximities will affect the observed buildup curves. Specifically, Fig. 8 presents corrected normalized experimental CHHC buildup curves (corresponding to $F^n_{LM}(t_{\mathrm{mix}})$ as defined in Eq. (19)) for magnetization starting on (a) C2, (b) C3, (c) C5 and (d) C8. As noted above, the data associated with single ^{1}H–^{1}H intramolecular contacts, i.e., C2–C4, C3–C5 and C5–C8 constitute *single-contact intramolecular reference curves*: The C2–C4, C3–C5 and C5–C8 peaks correspond to ^{1}H–^{1}H distances of 2.48 (H2–H4) and 2.47 Å (H3–H5) between neighboring aromatic protons and 2.56 Å (H5–H8) between an aromatic proton and the Cα proton. While all curves in Fig. 8 are converging to a similar plateau intensity at the longest experimental t_{mix} of 0.5 ms, differences in rate of buildup are clearly evident. Importantly, in agreement with the use of the CHHC experiment to identify structural constraints, it will be shown that the differences in buildup rate are directly related to the root-sum-square coupling, d_{rss}, [61–63] for the corresponding ^{1}H–^{1}H proximities (listed in Table 5):

$$d_{\mathrm{rss}} = \sqrt{\sum d_{jk}^2} \tag{29}$$

where the dipolar coupling constant, d_{jk}, is defined:

$$d_{jk} = \left(-\frac{\mu_0}{4\pi}\frac{\gamma_H^2\hbar}{r_{jk}^3}\right)/2\pi \tag{30}$$

The close resemblance between the C2–C*j* and C3–C*j* patterns in Fig. 8 reveals the presence of relatively similar proton environments around the H2 and H3 protons. In both cases, the upper limit is provided by the corresponding single-contact intramolecular reference curve (C2–C4 and C3–C5), while the lower limit is established by the contact with the H8 proton. The slower buildup of the C2–C8 and C3–C8 curves is consistent with the closest H–H proximity being over 4 Å (H2–H8: intermolecular 4.14 Å, H3–H8: intramolecular 4.75 Å). The remaining CHHC curves in the C2-C*j* and C3-C*j* patterns are distributed within the two limiting curves. As a common feature, all of them are encoding significant (in some cases multiple) intermolecular contributions, since their fast buildup is inconsistent with the large intramolecular ^{1}H–^{1}H distances (>4.5 Å). The C2–C3/C3–C2 buildup curve, determined by a single 2.9 Å intermolecular contact, is the only one that can be directly compared with the reference curve in terms of the encoded distances. Nevertheless, the difference between the C2–C7 and C3–C7 buildup curves is consistent with the difference in the corresponding average nearest proton–proton distances of 3.0 and 3.5 Å, respectively and d_{rss} = 10.1 and 4.6 kHz, respectively.

It is informative to compare the examples of the C2–C5 and C3–C4 buildup curves that correspond to multiple intermolecular proximities under 3.5 Å (H2–H5 2.76 and 3.19 Å, d_{rss} = 6.9 kHz;

Table 5
Proton-proton contacts shorter than 5 Å extracted from the crystal structure [60] of L-tyrosine·HCl[a]. Intramolecular contacts are shown in bold. The root-sum-square coupling, d_{rss}, (in kHz, see Eq. (29)) is given in square brackets (^{1}H nuclei within 5 Å are considered in the summations).

	H7	H8	H2	H3	H5	H4
H7 ($^{\beta}$CH$_2$)	–	(**2.50**; **3.06**) (2.93; 3.40) [10.5]	(**4.65**; >5) (2.31; 3.75) [10.1]	(**4.87**; >5) (3.44; 3.52) (3.95; >5) (4.68; >5) [4.6]	(**2.72**; **3.78**) (2.80; 2.93) [9.7]	(**3.50**; **2.33**) (4.15; >5) [10.1]
H8 ($^{\alpha}$CH)		–	>**5** 4.14 4.96 [1.8]	**4.75** 4.96 [1.5]	**2.56** >5 [7.2]	**4.45** 4.82 [1.7]
H2 (CH$_{\mathrm{arom}}$)			–	**4.29** 2.95 4.06 4.30 [5.5]	**4.96** 2.76 3.19 [6.9]	**2.48** 4.49 4.68 4.73 [8.2]
H3 (CH$_{\mathrm{arom}}$)				–	**2.47** 4.49 4.78 4.89 [8.3]	**4.93** 2.84 3.20 3.24 [7.4]
H5 (CH$_{\mathrm{arom}}$)					–	**4.28** 3.07 4.10 4.89 [4.9]
H4 (CH$_{\mathrm{arom}}$)						–

[a]The distinct ^{1}H nuclei are tabulated in the order of the corresponding ^{13}C resonances (increasing ppm).

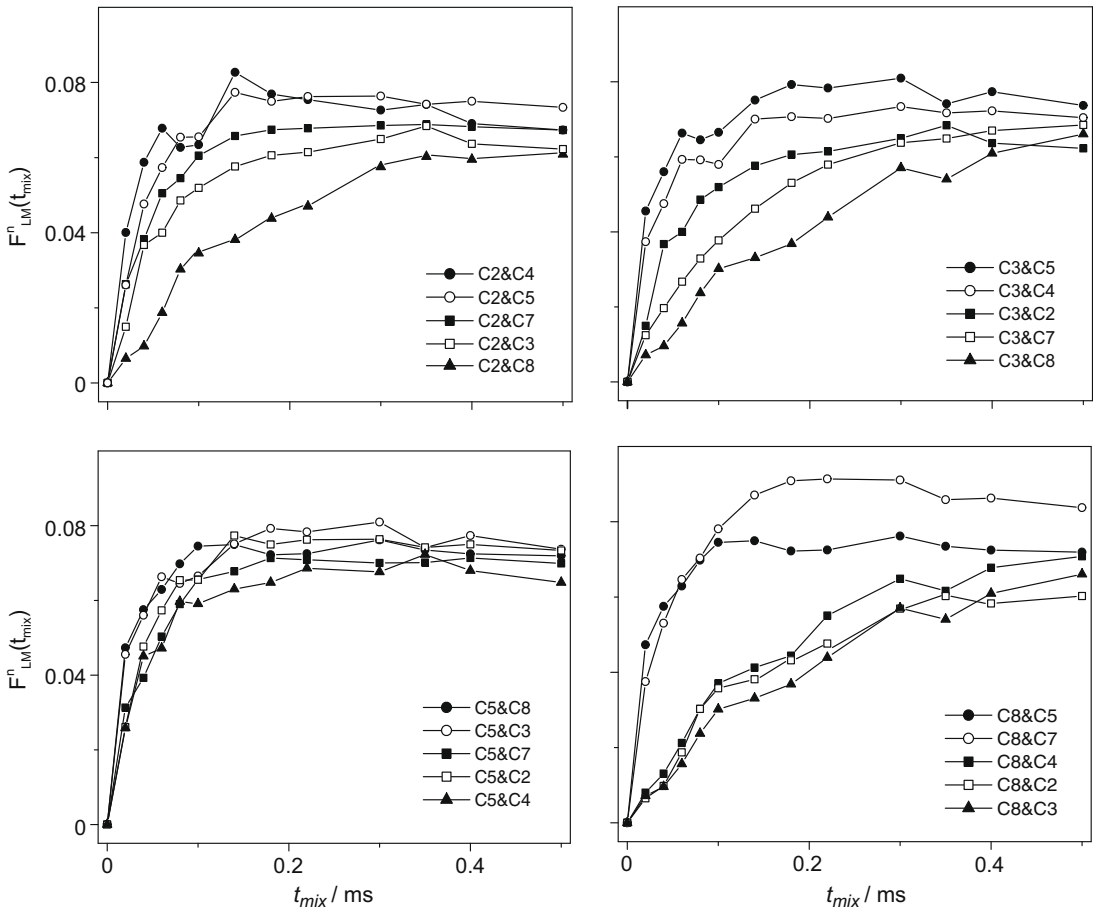

Fig. 8. Corrected normalized experimental CHHC buildup curves corresponding to $F^n_{LM}(t_{\mathrm{mix}})$ as defined in Eq. (19) for U–^{13}C L-tyrosine·HCl for magnetization starting on (a) C2, (b) C3, (c) C5 and (d) C8.

H3–H4 2.84, 3.20 and 3.24 Å, d_{rss} = 7.4 kHz) with the curves corresponding to single H–H proximities, i.e., the two intramolecular C2–C4 and C3–C5 reference curves and the C2–C3/C3–C2 single intermolecular contact, where the closest H–H distances are 2.48 Å (H2–H4), 2.47 Å (H3–H5) and 2.95 Å (H2–H3) and d_{rss} = 8.2 kHz (H2–H4), d_{rss} = 8.3 kHz (H3–H5) and d_{rss} = 5.5 kHz (H2–H3). The closeness of the C3–C4 and C3–C5 buildup curves is consistent with the similar d_{rss} values. The effect of multiple ^{1}H–^{1}H proximities leading to a faster buildup is evident when comparing the C2–C5 and C3–C4 curves on the one hand with the C2–C3 curve on the other hand.

A good correspondence between the experimental CHHC data and the corresponding structural parameters was found also for the C5–C*j* and C8–C*j* patterns in Fig. 8. Notably, C5–C*j* is representative for a ^{1}H site tightly coupled to its surrounding protons. Together with the intramolecular reference curves (C5–C3, C5–C8), the other three curves in this pattern also encode short intermolecular contacts, with ^{1}H–^{1}H distances between 2.8 and 3.1 Å and similar d_{rss} values (between 4.9 and 9.7 kHz). At the other extreme, the C8–C*j* pattern corresponds to strong couplings of H8 only with intramolecular protons, whereas all the intermolecular contacts are larger than 4 Å. This is clearly evidenced by the measured buildup curves.

4.5. Comparison of CHHC buildup data for U–^{13}C and U–^{13}C$^{\mathrm{dil_10\%}}$ samples

Fig. 9 compares corrected normalized buildup plots, i.e., $F^n_{LM}(t_{\mathrm{mix}})$, for U–^{13}C (circles) and U–^{13}C$^{\mathrm{dil_10\%}}$ (triangles) L-tyrosine·HCl for the cases where significant intensity (i.e., above the noise level) is observed for the U–^{13}C$^{\mathrm{dil_10\%}}$ sample. These cases (C2–C4, C3–C5, C4–C7, C5–C7, C5–C8 and C7–C8) all correspond to closest intramolecular H–H proximities under 3 Å, while for the other cases, the closest intramolecular H–H proximity is over 4 Å. In this context, while Fig. 8 shows CHHC buildup curves for the U–^{13}C sample involving C8 that correspond to closest H–H distances of over 4 Å, for the U–^{13}C$^{\mathrm{dil_10\%}}$ sample, it is to be remembered that much CHHC signal intensity is lost to invisible protons attached to ^{12}C nuclei at longer mixing times (see Fig. 7 and Section 4.3). Comparing the buildup curves for the U–^{13}C and U–^{13}C$^{\mathrm{dil_10\%}}$ samples in the short t_{mix} regime (<80 μs), it is observed that four of them (C2–C4, C3–C5, C4–C7, and C5–C8) are quite similar in shape, while for the C5–C7 and C7–C8 cases, faster buildup is observed for the U–^{13}C sample. As was discussed in Section 4.3 when comparing the CHHC data for C7–C8 and C2–C4 (see Fig. 6), this difference is a consequence of additional close H5–H7 and H7–H8 intermolecular proximities.

5. Summary and conclusions

CHHC-type experiments are being increasingly applied to indirectly probe ^{1}H–^{1}H magnetization exchange and hence obtain structural constraints, in particular, for large biomolecules. This paper has presented a protocol for correcting the effect of non-specific cross polarization in CHHC experiments, thus allowing the recovery of the ^{1}H–^{1}H magnetization exchange functions from the mixing-time dependent buildup of experimental CHHC peak intensity. The presented protocol also incorporates a scaling

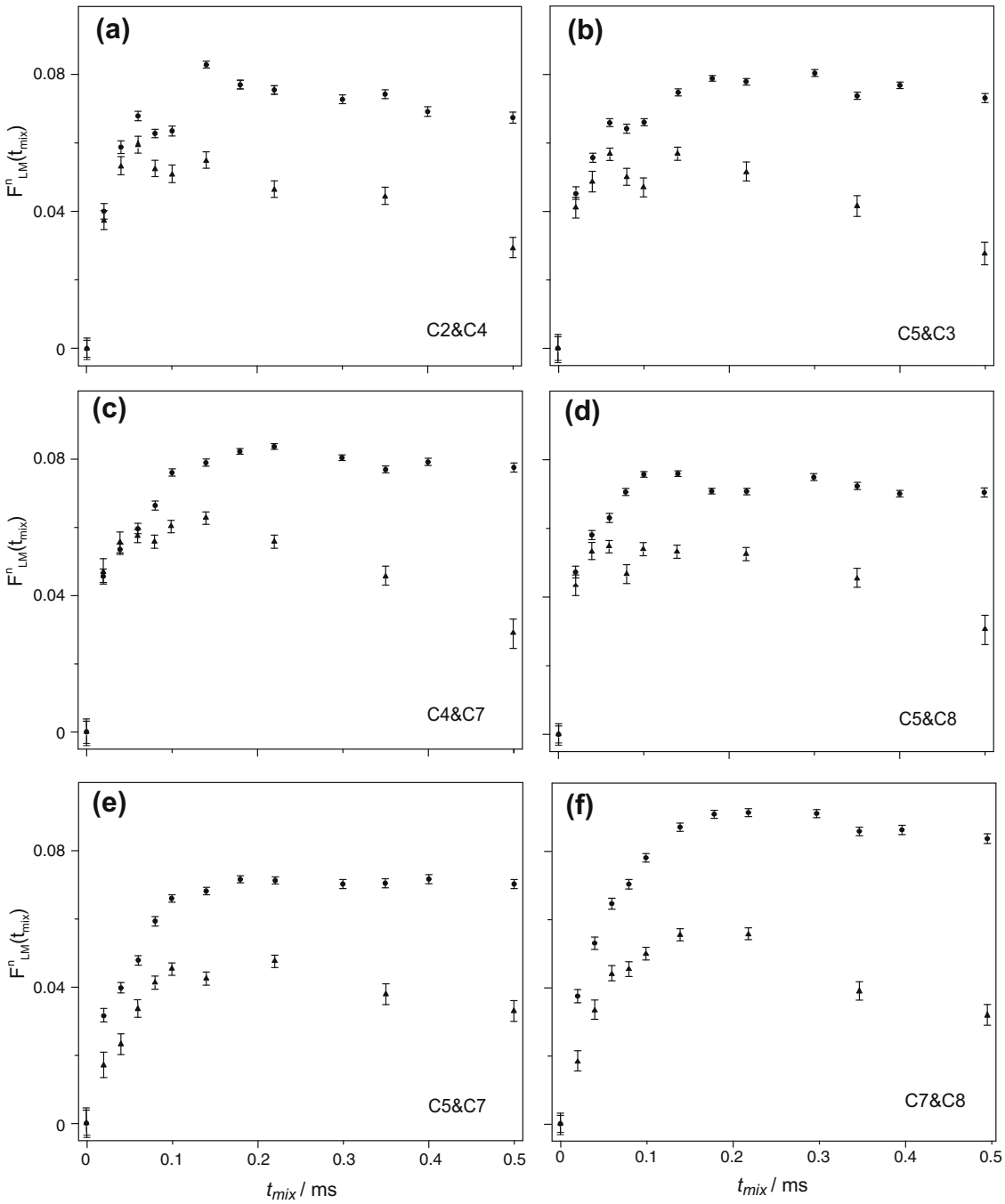

Fig. 9. Comparison between the corrected normalized experimental CHHC buildup curves, i.e., $F^n_{LM}(t_{mix})$ as defined in Eqs. (19) and (28), for U–^{13}C (circles) and U–$^{13}C^{dil_10\%}$ (triangles) L-tyrosine·HCl for (a) C2–C4, (b) C3–C5, (c) C4–C7, (d) C5–C8, (e) C5–C7 and (f) C7–C8.

procedure to take into account the effect of multiplicity of a CH_2 or CH_3 moiety. In this way, direct comparison can be made between experimentally determined ^{1}H–^{1}H magnetization exchange functions and numerical density-matrix simulations, without the requirement for any phenomenological factors. For L-tyrosine·HCl, good agreement between experiment and 11-spin simulation (including only isotropic ^{1}H chemical shifts) is demonstrated for the specific case of initial buildup ($t_{mix} < 100$ μs) of CHHC peak intensity corresponding to an intramolecular close (2.5 Å) H–H proximity. The derived corrections are not limited to the case of ^{1}H–^{1}H magnetization exchange, i.e., to zero-quantum mixing schemes, but they are also valid to CHHC experiments employing homonuclear ^{1}H–^{1}H recoupling schemes [17,50].

For small and moderately sized organic molecules such as L-tyrosine·HCl, the experimentally observed buildup of CHHC peak intensity often corresponds to a ^{1}H–^{1}H magnetization exchange behavior that depends on both intra and intermolecular proximities. Indeed, it is to be noted that the multi-spin kinetic rate matrix analysis of directly observed ^{1}H–^{1}H magnetization exchange by Elena et al. exploits the dependence on intermolecular ^{1}H–^{1}H proximities to determine the three-dimensional packing of organic molecules in the crystal lattice [22,23]. In the CHHC experiment, intermolecular effects can be removed by working with dilute samples where a U–^{13}C labeled molecule is recrystallised with an excess of molecules at natural abundance. This approach has been employed in previous studies where distance constraints extracted

from CHHC experiments have been used as constraints in the structural determination of the three-dimensional conformation of organic molecules [49–51]. In this paper, experimental CHHC buildup curves were presented for L-tyrosine·HCl samples where either all or only one in ten molecules are U–^{13}C labeled. For the dilute sample, CHHC cross-peak intensities tended to significantly lower values for long mixing times (500 μs) than for the 100% sample. This difference has been explained here as being due to the dependence of the limiting total magnetization on the ratio N_{obs}/N_{tot} between the number of protons that are directly attached to a ^{13}C nucleus and hence contribute significantly to the observed ^{13}C CHHC NMR signal, and the total number of ^{1}H spins into the system.

It has been shown that insight into ^{1}H–^{1}H magnetization exchange under multiple intra and intermolecular ^{1}H–^{1}H dipolar couplings can be obtained by a consideration of the root sum squared dipolar couplings corresponding to specific CHHC cross peaks. (Note that a sum squared dipolar coupling is also inherent to the multi-spin kinetic rate matrix analysis of directly observed ^{1}H–^{1}H magnetization exchange by Elena et al. [22,23]) ^{1}H–^{1}H magnetization exchange curves extracted from CHHC spectra for the 100% L-tyrosine·HCl sample exhibit a clear sensitivity to the root sum squared dipolar coupling, with fast buildup being observed for the shortest intramolecular distances (2.5 Å) and slower, yet observable buildup for the longer intermolecular distances (up to 5 Å). As is to be expected, differences in the initial CHHC buildup were observed between the 1 in 10 dilute and 100% samples for cases where there is a close intermolecular H–H proximity in addition to a close intramolecular H–H proximity. The demonstrated usefulness of the CHHC experiment as a valuable and reliable source of quantitative H–H proximity information is consistent with previous studies of other small organic molecules [50,51] as well the microcrystalline CrH protein [30], for which ^{1}H–^{1}H distances are known from single-crystal diffraction data.

Of much current interest is the application of CHHC-type experiments, including the recently developed J-CHHC [64], to large biomolecules, where extracted ^{1}H–^{1}H distances are then used as constraints in structural determination protocols [29,31,32,36,37,44,46,64]. For large biomolecules, the ^{1}H–^{1}H magnetization exchange as encoded in CHHC-type peaks is less complex than in the case of small and moderately sized molecules since intermolecular ^{1}H–^{1}H proximities do not usually contribute, although NHHC experiments have been used to probe inter monomer contacts for the CrH microcrystalline protein [30]. As noted above, it has been shown here that good agreement between experiment and 11-spin simulation (including only isotropic ^{1}H chemical shifts) was observed for the initial buildup (t_{mix} < 100 μs) of CHHC peak intensity corresponding to a single intramolecular H–H proximity. For large biomolecules, most CHHC-type peaks usually correspond to such single intramolecular H–H proximities, thus suggesting that an analysis of CHHC-type buildup curves (using the protocol presented here to correct for non-specific CP and take into account XH_n multiplicity) using multi-spin simulations could be utilized to check and refine H–H distances in as-determined biomolecular structures.

Acknowledgments

Financial support from the ANCS. NIH (grants EB-001960, EB-003151 and EB-002026), EPSRC, and the Royal Society is gratefully acknowledged. Tim Smith and Andrew Marsh (Warwick) are thanked for assistance with sample preparation.

Appendix A

Representative SPINEVOLUTION input files used for the numerical simulation of the $F_{jk}(t_{mix})$ polarization transfer functions in Eq. (1).

```
******The System***********************************
spectrometer (MHz)                                   400
spinning_freq (kHz)                                  10
channels                                             H1
nuclei                                               H1 H1 H1 H1 H1 H1 H1 H1 H1 H1 H1
atomic_coords                                        cross87_d.cor
cs_isotropic                                         3 2.8 4.5 8 8 8 7 7 7 7 3 ppm
csa_parameters                                       *
j_coupling                                           *
quadrupole                                           *
dip_switchboard                                      *
csa_switchboard                                      *
exchange_nuclei                                      (4 5 6)
bond_len_nuclei                                      *
bond_ang_nuclei                                      *
tors_ang_nuclei                                      *
groups_nuclei                                        *

*******Pulse Sequence*****************************
CHN 1
timing (usec)                                        (5)200
power (kHz)                                          0
phase (deg)                                          0
freq_offs (kHz)                                      0
phase_cycling                                        * * (RCV)

*************************Variables ***************************Options etc ************************************
rho0                                                 1 1 0 0 0 0 0 0 0 0 0 Iz
observed_spins                                       1 2 3 4 5 6 7 8 9 10 11 Iz
```

(continued on next page)

Appendix A (*continued*)

EulerAngles	repl00.dat
n_gamma	l0
line_broaden (Hz)	*
zerofill	*
FFT_dimensions	*
cross87_d.cor	
8.207 −0.698 −0.686	H7a(CH2 − molecule A)
8.554 0.898 −1.274	H7b(CH2 − A)
7.034 0.260 1.303	H8(CH − A)
5.976 1.412 −1.213	Ha(NH3 − A)
5.169 0.883 0.100	Hb(NH3 − A)
5.951 −0.187 −0.894	Hc(NH3 − A)
10.630 1.831 −0.798	H4(CHring − A)
9.091 −1.154 1.852	H5(CHring − A)
9.394 −2.663 −0.444	H2(CHring inter − C)
9.253 −1.154 −3.245	H5(CHring inter − B)
7.196 0.260 −3.793	H8(CH − B)

References

[1] J. Pauli, M. Baldus, B. Van Rossum, H. De Groot, H. Oschkinat, Backbone and side-chain ^{13}C and ^{15}N signal assignments of the α-spectrin SH3 domain by magic angle spinning solid-state NMR at 17.6 Tesla, ChemBioChem 2 (2001) 272–281.

[2] M. Hohwy, C.M. Rienstra, R.G. Griffin, Band-selective homonuclear dipolar recoupling in rotating solids, J. Chem. Phys. 117 (2002) 4973–4987.

[3] C.P. Jaroniec, C. Filip, R.G. Griffin, 3D TEDOR NMR experiments for the simultaneous measurement of multiple carbon–nitrogen distances in uniformly ^{13}C,^{15}N-labeled solids, J. Am. Chem. Soc. 124 (2002) 10728–10742.

[4] A.T. Petkova, M. Baldus, M. Belenky, M. Hong, R.G. Griffin, J. Herzfeld, Backbone and side chain assignment strategies for multiply labeled membrane peptides and proteins in the solid state, J. Magn. Reson. 160 (2003) 1–12.

[5] V. Ladizhansky, C.P. Jaroniec, A. Diehl, H. Oschkinat, R.G. Griffin, Measurement of multiple ψ torsion angles in uniformly ^{13}C,^{15}N-labeled α-spectrin SH3 domain using 3D ^{15}N–^{13}C–^{13}C–^{15}N MAS dipolar-chemical shift correlation spectroscopy, J. Am. Chem. Soc. 125 (2003) 6827–6833.

[6] P.T.F. Williamson, A. Verhoeven, M. Ernst, B.H. Meier, Determination of internuclear distances in uniformly labeled molecules by rotational-resonance solid-state NMR, J. Am. Chem. Soc. 125 (2003) 2718–2722.

[7] V. Ladizhansky, R.G. Griffin, Band-selective carbonyl to aliphatic side chain ^{13}C–^{13}C distance measurements in U–^{13}C,^{15}N-labeled solid peptides by magic angle spinning NMR, J. Am. Chem. Soc. 126 (2004) 948–958.

[8] C.P. Jaroniec, C.E. MacPhee, V.S. Bajaj, M.T. McMahon, C.M. Dobson, R.G. Griffin, High-resolution molecular structure of a peptide in an amyloid fibril determined by magic angle spinning NMR spectroscopy, PNAS 101 (2004) 711–716.

[9] K. Seidel, A. Lange, S. Becker, C.E. Hughes, H. Heise, M. Baldus, Protein solid-state NMR resonance assignments from (^{13}C,^{13}C) correlation spectroscopy, PCCP 6 (2004) 5090–5093.

[10] H. Heise, K. Seidel, M. Etzkorn, S. Becker, M. Baldus, 3D NMR spectroscopy for resonance assignment and structure elucidation of proteins under MAS: novel pulse schemes and sensitivity considerations, J. Magn. Reson. 173 (2005) 64–74.

[11] A.B. Siemer, C. Ritter, M.O. Steinmetz, M. Ernst, R. Riek, B.H. Meier, ^{13}C,^{15}N Resonance assignment of parts of the HET-s prion protein in its amyloid form, J. Biomol. NMR 35 (2006) 75–87.

[12] A. Grommek, B.H. Meier, M. Ernst, Distance information from proton-driven spin diffusion under MAS, Chem. Phys. Lett. 427 (2006) 404–409.

[13] F. Castellani, B. Van Rossum, A. Diehl, M. Schubert, K. Rehbein, H. Oschkinat, Structure of a protein determined by solid-state magic-angle-spinning NMR spectroscopy, Nature 420 (2002) 98–102.

[14] S. Zhang, B.H. Meier, R.R. Ernst, Polarization echoes in NMR, Phys. Rev. Lett. 69 (1992) 2149–2151.

[15] M. Wilhelm, H. Feng, U. Tracht, H.W. Spiess, 2D CP/MAS ^{13}C isotropic chemical shift correlation established by ^{1}H spin diffusion, J. Magn. Reson. 134 (1998) 255–260.

[16] F.M. Mulder, W. Heinen, M. van Duin, J. Lugtenburg, H.J.M. de Groot, Spin diffusion with ^{13}C selection and detection for the characterization of morphology in labeled polymer blends with MAS NMR, J. Am. Chem. Soc. 120 (1998) 12891–12894.

[17] A. Lange, S. Luca, M. Baldus, Structural constraints from proton-mediated rare spin correlation spectroscopy in rotating solids, J. Am. Chem. Soc. 124 (2002) 9704–9705.

[18] P. Caravatti, P. Neuenschwander, R.R. Ernst, Characterization of heterogeneous polymer blends by two-dimensional proton spin diffusion spectroscopy, Macromolecules 18 (1985) 119–122.

[19] F. Babonneau, V. Gualandris, J. Maquet, D. Massiot, M.T. Janicke, B.F. Chmelka, Newly applied two-dimensional solid-state NMR correlation techniques for the characterization of organically modified silicates, J. Sol–Gel Sci. Technol. 19 (2000) 113–117.

[20] G.R. Goward, M.F.H. Schuster, D. Sebastiani, I. Schnell, H.W. Spiess, High-resolution solid-state NMR studies of imidazole-based proton conductors: structure motifs and chemical exchange, J. Phys. Chem. B 106 (2002) 9322–9334.

[21] J. Brus, H. Petrickova, J. Dybal, Influence of local molecular motions on the determination of ^{1}H–^{1}H Internuclear distances measured by 2D ^{1}H spin-exchange experiments, Solid State Nucl. Magn. Reson. 23 (2003) 183–197.

[22] B. Elena, L. Emsley, Powder crystalography by proton solid-state NMR spectroscopy, J. Am. Chem. Soc. 127 (2005) 9140–9146.

[23] B. Elena, G. Pintacuda, N. Mifsud, L. Emsley, Molecular structure determination in powders by NMR crystallography from proton spin diffusion, J. Am. Chem. Soc. 128 (2006) 9555–9560.

[24] S.P. Brown, Probing proton–proton proximities in the solid state, Progr. Nucl. Magn. Reson. Spectrosc. 50 (2007) 199–251.

[25] Y. Wei, A. Ramamoorthy, 2D ^{15}N–^{15}N isotropic chemical shift correlation established by ^{1}H–^{1}H dipolar coherence transfer in biological solids, Chem. Phys. Lett. 342 (2001) 312–316.

[26] D. Massiot, B. Alonso, F. Fayon, F. Fredoueil, B. Bujoli, New NMR developments for structural investigations of proton-bearing materials at different length scales, Sol. St. Sci. 3 (2001) 11–16.

[27] B. Reif, B.J. van Rossum, F. Castellani, K. Rehbein, A. Diehl, H. Oschkinat, Characterization of ^{1}H–^{1}H distances in a uniformly ^{2}H,^{15}N-labeled SH3 domain by MAS solid-state NMR spectroscopy, J. Am. Chem. Soc. 125 (2003) 1488–1489.

[28] M. Etzkorn, A. Böckmann, A. Lange, M. Baldus, Probing molecular interfaces using 2D magic-angle-spinning NMR on protein mixtures with different uniform labeling, J. Am. Chem. Soc. 126 (2004) 14746–14751.

[29] K. Seidel, M. Etzkorn, H. Heise, S. Becker, M. Baldus, High-resolution solid-state NMR studies on U[^{13}C,^{15}N]-labeled ubiquitin, ChemBioChem 6 (2005) 1638–1647.

[30] C. Gardiennet, A. Loquet, M. Etzkorn, H. Heise, M. Baldus, A. Bockmann, Structural constraints for the Crh protein from solid-state NMR experiments, J. Biomol. NMR 40 (2008) 239–250.

[31] A. Loquet, B. Bardiaux, C. Garninnet, C. Blanchet, M. Baldus, M. Nilges, T. Maliavin, A. Bockmann, 3D structure determination of the Crh protein from highly ambiguous solid-state NMR restraints, J. Am. Chem. Soc. 130 (2008) 3579–3589.

[32] W.T. Franks, B.J. Wylie, H.L. Frericks Schmidt, A.J. Nieuwkoop, R.M. Mayrhofer, G.J. Shah, D.T. Graesser, C.M. Rienstra, Dipole tensor-based atomic-resolution structure determination of a nanocrystalline protein by solid-state NMR, PNAS 105 (2008) 4621–4626.

[33] R. Tycko, Y. Ishii, Constraints on supramolecular structure in amyloid fibrils from two-dimensional solid-state NMR spectroscopy with uniform isotopic labelling, J. Am. Chem. Soc. 125 (2003) 6606–6607.

[34] A.T. Petkova, G. Buntkowsky, F. Dyda, R.D. Leapman, W.-M. Yau, R. Tycko, Solid state NMR reveals a pH-dependent antiparallel β-sheet registry in fibrils formed by a β-amyloid peptide, J. Mol. Biol. 335 (2004) 247–260.

[35] H. Heise, W. Hoyer, S. Becker, O.C. Andronesi, D. Riedel, M. Baldus, Molecular-level secondary structure, polymorphism, and dynamics of full-length of α-synuclein fibrils studied by solid-sate NMR, PNAS 102 (2005) 15871–15876.

[36] K. Iwata, T. Fujiwara, Y. Matsuki, H. Akutsu, S. Takahashi, H. Naiki, Y. Goto, 3D structure of amyloid protofilaments of beta2 micro-globulin fragment probed by solid-state NMR, PNAS 103 (2006) 18119–18124.

[37] C. Wasmer, A. Lange, H. Van Melckebeke, A.B. Siemer, R. Riek, B.H. Meier, Amyloid fibrils of the HET-s (218-289) prion form a β solenoid with a triangular hydrophobic core, Science 319 (2008) 1523–1526.
[38] M. Tang, A.J. Waring, M. Hong, Intermolecular packing and alignment in an ordered β-hairpin antimicrobial peptide aggregate from 2D solid state NMR, J. Am. Chem. Soc. 127 (2005) 13919–13927.
[39] O.C. Andronesi, M. Von Bergen, J. Biernat, K. Seidel, C. Griesinger, E. Mandelkow, M. Baldus, Characterization of Alzheimer's-like paired helical filaments from the core domain of Tau protein using solid-state NMR spectroscopy, J. Am. Chem. Soc. 130 (2008) 5922–5928.
[40] I. de Boer, L. Bosman, J. Raap, H. Oschkinat, H.J.M. de Groot, 2D ^{13}C–^{13}C MAS NMR correlation spectroscopy with mixing by true ^{1}H spin diffusion reveals long-range intermolecular distance restraints in ultra high magnetic field, J. Magn. Reson. 157 (2002) 286–291.
[41] I. de Boer, J. Matysik, M. Amakawa, S. Yagai, H. Tamiaki, A.R. Holzwarth, H.J.M. de Groot, MAS NMR structures of a microcrystalline Cd-bacteriochlorophyll d-analog, J. Am. Chem. Soc. 125 (2003) 13374–13375.
[42] I. de Boer, J. Matysik, K. Erkelens, S. Sasaki, T. Miyatake, S. Yagai, H. Tamiaki, A.R. Holzwarth, H.J.M. de Groot, MAS NMR structures of aggregated cadmium chlorins reveal molecular control of self-assembly of chlorosomal bacteriochlorophylls, J. Phys. Chem. B 108 (2004) 16566.
[43] S. Ganapathy, A.J. van Gammeren, F.B. Hulsbergen, H.J.M. de Groot, Probing secondary, tertiary, and quaternary structure along with protein–cofactor interactions for a helical transmembrane protein complex through ^{1}H spin diffusion with MAS NMR spectroscopy, J. Am. Chem. Soc. 129 (2007) 1504–1505.
[44] A. Lange, S. Becker, K. Seidel, K. Giller, O. Pongs, M. Baldus, A concept for rapid protein–structure determination by solid-state NMR spectroscopy, Angew. Chem. Int. Ed. 44 (2005) 2089–2092.
[45] W. Luo, X. Yao, M. Hong, Large structure rearrangement of colicin ia channel domain after membrane binding from 2D ^{13}C spin diffusion NMR, J. Am. Chem. Soc. 127 (2005) 6402–6408.
[46] A. Lange, K. Giller, S. Hornig, M.F. Martin-Eauclaire, O. Pongs, S. Becker, M. Baldus, Toxin-induced conformational changes in a potassium channel revealed by solid-state NMR, Nature 440 (2006) 959–962.
[47] K. Riedel, J.Leppert.O. Ohlenschlager, M. Gorlach, R. Ramachandran, Characterisation of hydrogen bonding networks in RNAs via magic angle spinning solid state NMR, J. Biomol. NMR 31 (2005) 331–336.
[48] K. Riedel, C. Herbst, S. Hafner, J. Leppert, O. Ohlenschläger, M.S. Swanson, M. Görlach, R. Ramachandran, Constraints on the structure of $(CUG)_{97}$ RNA from magic-angle-spinning solid-state NMR spectroscopy, Angew. Chem. Int. Ed. 45 (2006) 5620–5623.
[49] A. Lange, T. Schupp, F. Petersen, T. Carlomagno, M. Baldus, High-Resolution Solid-State NMR Structure of an Anticancer Agent, ChemMedChem 2 (2007) 522–527.
[50] A. Lange, S. Luca, M. Baldus, Analysis of proton–proton transfer dynamics in rotating solids and their use for 3D structure determination, J. Am. Chem. Soc. 125 (2003) 126410–126418.
[51] K. Seidel, M. Etzkorn, L. Sonnenberg, C. Griesinger, A. Sebald, M. Baldus, Studying molecular 3D structure and dynamics by high-resolution solid-state NMR: application to L-tyrosine-ethylester, J. Phys. Chem. A 109 (2005) 2436–2442.
[52] M.H. Levitt, D.P. Raleigh, F. Creuzet, R.G. Griffin, Theory and simulations of homonuclear spin pair systems in rotating solids, J. Chem. Phys. 92 (1990) 6347.
[53] D. Suter, R.R. Ernst, Spin diffusion in resolved solid-state NMR spectra, Phys. Rev. B 32 (1985) 5608–5627.
[54] A. Kubo, C.A. McDowell, Spectral spin-diffusion in polycrystalline solids under magic-angle spinning, J. Chem. Soc. Faraday Trans. 84 (1988) 3713–3730.
[55] M. Veshtort, R.G. Griffin, SPINEVOLUTION: a powerful tool for the simulation of solid and liquid state NMR experiments, J. Magn. Reson. 178 (2006) 248–282.
[56] V. Zorin, M. Ernst, S.P. Brown, P. Hodgkinson, Insights into homonuclear decoupling from efficient numerical simulation: techniques and examples, J. Magn. Res. 192 (2008) 183–196.
[57] X. Filip, C. Tripon, C. Filip, Heteronuclear decoupling under fast MAS by a rotor-syncronized Hahn-Echo pulse train, J. Magn. Res. 176 (2005) 239–243.
[58] J.M. Griffin, C. Tripon, A. Samoson, C. Filip, S.P. Brown, Low-load rotor-synchronized Hahn-Echo pulse train (RS-HEPT) ^{1}H decoupling in solid-state NMR: factors affecting MAS spin-Echo dephasing time, Magn. Reson. Chem. 45 (2007) S198–S208.
[59] A.E. Bennett, C.M. Rienstra, M. Auger, K.V. Lakhsmi, R.G. Griffin, Heteronuclear decoupling in rotating solids, J. Chem. Phys. 123 (1995) 6951–6958.
[60] M.N. Frey, T.F. Koetzle, M.S. Lehmann, W.C. Hamilton, Precision neutron diffraction structure determination of protein and nucleic acid components. X. A comparison between the crystal and molecular structures of L-tyrosine and L-tyrosine hydrochloride, J. Chem. Phys. 58 (1973) 2547–2556.
[61] C. Filip, S. Hafner, I. Schnell, D.E. Demco, H.W. Spiess, Solid-state nuclear magnetic resonance spectra of dipolar-coupled multi-spin system under magic angle spinning, J. Chem. Phys. 110 (1999) 423–440.
[62] V.E. Zorin, S.P. Brown, P. Hodgkinson, Quantification of homonuclear dipolar coupling networks from magic-angle spinning ^{1}H NMR, Mol. Phys. 104 (2006) 293–304.
[63] V.E. Zorin, S.P. Brown, P. Hodgkinson, Origins of linewidth in ^{1}H magic-angle spinning NMR, J. Chem. Phys. 125 (2006) 144508.
[64] A. Loquet, S. Laage, C. Gardiennet, B. Elena, L. Emsley, A. Bőckmann, A. Lesage, Methyl proton contacts obtained using heteronuclear through-bond transfers in solid-state NMR spectroscopy, J. Am. Chem. Soc. 130 (2008) 10625–10632.